Mutating the Tight-Dimer Interface of Dihydrodipicolinate Synthase Disrupts the Enzyme Quaternary Structure: Toward a Monomeric Enzyme[†,‡]

F. Grant Pearce,[*,§] Renwick C. J. Dobson,[§,||] Anke Weber,[§] Laura A. Lane,[⊥] Margaret G. McCammon,[⊥] Marie A. Squire,[#] Matthew A. Perugini,[||] Geoffrey B. Jameson,[▽] Carol V. Robinson,[⊥] and Juliet A. Gerrard[*,§]

School of Biological Sciences, University of Canterbury, Private Bag 4800, Christchurch 8020, New Zealand, Bio21 Molecular Science and Biotechnology Institute and the Department of Biochemistry and Molecular Biology, The University of Melbourne, Melbourne, Victoria 3010, Australia, The University Chemical Laboratory, University of Cambridge, Lensfield Road, Cambridge CB2 1EW, U.K., Department of Chemistry, University of Canterbury, Private Bag 4800, Christchurch 8020, New Zealand, and Centre for Structural Biology, Institute of Fundamental Sciences, Massey University, Palmerston North, New Zealand

Received June 10, 2008; Revised Manuscript Received September 15, 2008

ABSTRACT: Dihydrodipicolinate synthase (DHDPS) is a tetrameric enzyme that is the first enzyme unique to the (*S*)-lysine biosynthetic pathway in plants and bacteria. Previous studies have looked at the important role of Tyr107, an amino acid residue located at the tight-dimer interface between two monomers, in participating in a catalytic triad of residues during catalysis. In this study, we examine the importance of this residue in determining the quaternary structure of the DHDPS enzyme. The Tyr107 residue was mutated to tryptophan, and structural, biophysical, and kinetic studies were carried out on the mutant enzyme. These revealed that while the solid-state structure of the mutant enzyme was largely unchanged, as judged by X-ray crystallography, it exists as a mixture of primarily monomer and tetramer in solution, as determined by analytical ultracentrifugation, size-exclusion chromatography, and mass spectrometry. The catalytic ability of the DHDPS enzyme was reduced by the mutation, which also allowed the adventitious binding of α-ketoglutarate to the active site. A reduction in the apparent melting temperature of the mutant enzyme was observed. Thus, the tetrameric quaternary structure of DHDPS is critical to controlling specificity, heat stability, and intrinsic activity.

In the synthesis of (*S*)-lysine in plants and bacteria, dihydrodipicolinate synthase (DHDPS,[1] EC 4.2.1.52) is located at the branch point of the pathway and, in most species studied to date, is feedback-regulated by (*S*)-lysine. It is, therefore, of interest as a target for antibiotics, herbicides, and pesticides (*1, 2*) and also as a control point for (*S*)-lysine biosynthesis, since lysine is often a limiting nutrient in staple crops (*3*). DHDPS catalyzes the condensation of (*S*)-aspartate β-semialdehyde [(*S*)-ASA] and pyruvate to form an unstable heterocyclic product, thought to be (4*S*)-4-hydroxy-2,3,4,5-tetrahydro-(2*S*)-dipicolinic acid (HTPA) (*4*).

(*S*)-Lysine biosynthesis is controlled at two points in the biosynthetic pathway (*5*). Regulation of the aspartate kinase enzyme can be used to control the synthesis of all of the aspartate family of amino acids, whereas regulation of DHDPS specifically controls the synthesis of (*S*)-lysine. As such, DHDPS is generally feedback-inhibited by (*S*)-lysine, with plant enzymes being strongly inhibited (*6*−*8*), DHDPS from Gram-negative bacteria being weakly inhibited (*9*−*11*), and DHDPS from Gram-positive bacteria and *Thermotoga maritima* showing little to no inhibition (*12*−*15*). (*S*)-Lysine inhibits *Escherichia coli* DHDPS as a mixed partial inhibitor with respect to pyruvate and a partial noncompetitive inhibitor with respect to (*S*)-ASA (*10*).

The active site of DHDPS has been well characterized and involves a catalytic triad of amino acid residues (*4, 10, 16*). Initially, pyruvate forms a Schiff base with Lys161, followed by the binding of (*S*)-ASA and subsequent dehydration and cyclization to form HTPA. The catalytic triad of Tyr133 and Thr44 from one subunit and Tyr107 from the second subunit acts as a proton shuttle to transfer protons to and from the active site (*10*).

Structural features of DHDPS have been well characterized, with the enzyme consisting of a homotetramer that is made up of a dimer of "tight dimers". Interestingly, the quaternary structure is different for the bacterial and plant enzymes, with *E. coli* (*17*) and *T. maritima* (*15*) sharing with *Nicotiana sylvestris* the tight-dimer arrangement but having a different arrangement of dimers to form the tetramer (*18*).

[†] This work was funded, in part, by the Royal Society of New Zealand, Marsden Fund, and, in part, by the Foundation of Research, Science and Technology via a fellowship to F.G.P. J.A.G., M.A.P., and R.C.J.D. acknowledge the DTRA basic research fund (AB07CBT004) and the ARC for part funding.

[‡] The coordinate and structure factor files were deposited with the RCSB Protein Data Bank with accession code 3DEN.

* Corresponding authors. E-mail: grant.pearce@canterbury.ac.nz or juliet.gerrard@canterbury.ac.nz. Tel: +64 3 364 2987ext 2987. Fax: +64 3 364 2590.

[§] School of Biological Sciences, University of Canterbury.

[||] The University of Melbourne.

[⊥] University of Cambridge.

[#] Department of Chemistry, University of Canterbury.

[▽] Massey University.

[1] Abbreviations: (*S*)-ASA, (*S*)-aspartate β-semialdehyde; CD, circular dichroism; DHDPR, dihydrodipicolinate reductase; DHDPS, dihydrodipicolinate synthase; HTPA, (4*S*)-4-hydroxy-2,3,4,5-tetrahydro-(2*S*)-dipicolinic acid.

10.1021/bi801094t CCC: $40.75
Published on Web 10/21/2008

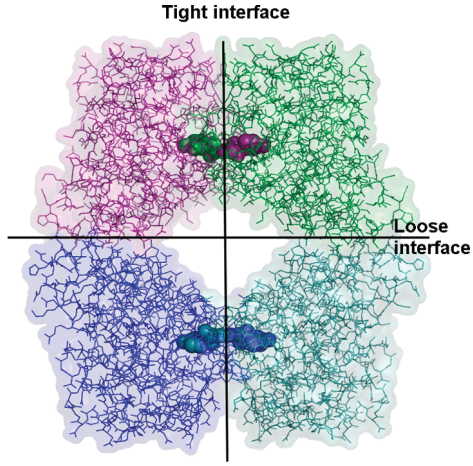

FIGURE 1: Tyr107 is located at the "tight-dimer" interface, with the side chain reaching into the active site of the other monomer.

Recent studies have shown that the DHDPS enzyme from methicillin-resistant *Staphylococcus aureus* exists in a monomer−dimer equilibrium but has similar activity to the *E. coli* tetramer (*19*).

The active site is located at the C-terminal end of the $(\alpha/\beta)_8$ barrel, near the tight-dimer interface, with Tyr106 from one monomer forming an aromatic stack with Tyr107 from the corresponding monomer (Figure 1). Previous studies have shown that mutation of Tyr107 to phenylalanine substantially reduced the catalytic activity but caused only very minor differences to the crystal structure and left the solution-state tetrameric structure intact (*20*).

As part of our investigations into the potential for targeting quaternary structure as a paradigm for drug design (*21*), we are interested in disrupting the interfaces of DHDPS and generating dimeric and monomeric species in order to explore the role of quaternary structure in enzyme function. Recently, we have engineered dimeric variants of the DHDPS enzyme which, despite conserved active site architecture, show reduced catalytic activity and a propensity to form a covalent adduct with adventitious α-ketoglutarate (*22*). As a continuation of these studies, Tyr107 of *E. coli* DHDPS was mutated to a more bulky tryptophan residue using site-directed mutagenesis, and a complete characterization of the resulting enzyme is reported herein.

EXPERIMENTAL PROCEDURES

Materials. Unless otherwise stated, all chemicals were obtained from Sigma Chemical Co., GE Biosciences, or Invitrogen. Protein concentration was measured by the method of Bradford (*23*). Enzymes were manipulated at 4 °C or on ice. (*S*)-ASA was synthesized using the methods of Roberts et al. (*24*) and was of high quality (>95%) as judged by ^{1}H NMR and the coupled assay to dihydrodipicolinate reductase (DHDPR) (*2, 9*). DHDPR from *E. coli* was purified by previously reported methods (*10, 25*).

Cloning, Overexpression, and Purification. Mutations in the *dap*A gene encoding *E. coli* DHDPS were introduced to the pJG001 plasmid (*10*) using the QuickChange site-directed mutagenesis kit (Stratagene). Reaction conditions were carried out following the manufacturer's instructions, and the mutation was confirmed by sequencing. The mutant form of the enzyme was expressed in *dap*A-negative *E. coli* AT997r$^-$ and purified as previously described (*10*). Labeled enzyme was produced by growing cells in minimal media supplemented with [^{13}C]glucose and [^{15}N]ammonium chloride.

Table 1: Data Collection and Refinement Statistics

no. of images	348
oscillation range (deg)	0.2
unit cell	
a, *b*, *c* (Å)	121.20, 121.20, 110.57
α, *β*, *γ* (deg)	90, 90, 120
processing resolution (Å) (outer shell)	32.22−2.20 (2.257−2.20)
no. of reflections/unique	214054/45134
completeness (%)	100 (100)
R_{merge}	0.084 (0.412)
$I/\sigma(I)$	9.49 (3.2)
refinement resolution (Å)	2.20 (2.26−2.20)
R_{free}	0.234 (0.318)
R_{cryst}	0.188 (0.249)
mean *B* value (Å)	29.4
solvent molecules	450
rms deviation	
bond lengths (Å)	0.012
bond angles (deg)	1.42

Crystallization and X-ray Data Collection. Crystallization experiments were performed as described (*17*) using the hanging-drop vapor diffusion method at 12 °C. Each drop contained protein (5 mg·mL^{-1} (160 μM) in 20 mM Tris-HCl, pH 8.0, 2.5 μL), precipitant (1.8 M K_2HPO_4, pH 10, 1.2 μL), and *n*-octyl *β*-D-glucopyranoside (6% w/v, 0.6 μL). Crystals appeared after 3 days and grew to dimensions of up to 0.3 mm. For X-ray diffraction data collection, crystals were soaked in cryoprotectant solution (2.0 M K_2HPO_4, pH 10.1, 20% v/v glycerol) and flash frozen in liquid nitrogen. Intensity data were collected at 110 K using an RAxisIV++ image plate detector coupled to a Rigaku Micromax-007 X-ray generator operating at 40 kV and 20 mA. The crystals belonged to space group $P3_121$ and diffracted to beyond 2.0 Å resolution. Diffraction data sets were processed and scaled using the package CrystalClear (*26*).

Structure Determination and Refinement. The orientation and location of each DHDPS mutant structure were determined using molecular replacement (AMoRe (*27*)), where the search model was the *E. coli* DHDPS monomer 1YXC (*28*). The asymmetric unit contained two monomers, and refinement was achieved using Refmac5 (*29*) with manual model corrections using the program Coot (*30*). The final refinement rounds involved the placement of solvent molecules using Arp (*31*) and inclusion of an α-ketoglutarate attached to Lys161. Dataman (*32*) was used to transfer the R_{free} flags from the wild-type *E. coli* data set to the mutant data sets prior to any refinement of the structure. Procheck (*33*) and the validation tools in Coot (*30*) were used to examine the quality of the final structure. A total of 94.1% of the residues fell into the most favored regions of the Ramachandran plot, 5.5% into the additional allowed region, and 0.4% (Trp107) into the disallowed region. Data collection and model refinement statistics are summarized in Table 1. The coordinate and structure factor files were deposited with the RCSB Protein Data Bank with accession code 3DEN. Images in this work were produced with Pymol (http://www.pymol.org).

Analytical Ultracentrifugation. Sedimentation experiments were performed in a Beckman Coulter Model XL-I analytical ultracentrifuge equipped with UV/vis scanning optics and

an An-60 Ti 4-hole rotor. Protein sample and reference (20 mM Tris-HCl, 150 mM NaCl, pH 8.0) solutions were loaded into 12 mm double-sector cells with quartz windows. For sedimentation velocity experiments, samples at an initial protein concentration of 1.6, 4.8, and 16 μM (380 μL) and reference (400 μL) were centrifuged at 40000 rpm at 20 °C, and data were collected in continuous mode at 230 or 233 nm without averaging. Data were fitted to a continuous size-distribution model (*34*) using the program SEDFIT (which is available from www.analyticalultracentrifugation.com) employing $P = 0.95$ and a resolution of 100 species ranging from 0.5 to 10 S for $c(s)$ distribution analysis or 3000 to 300000 Da for $c(M)$ distribution analysis. The partial specific volume ($\bar{\nu}$) of the sample (0.7407 mL·g^{-1}), buffer density (1.005 g·mL^{-1}), and buffer viscosity (1.021 cP) were computed using the program SEDNTRP (*35*).

For sedimentation equilibrium experiments, samples (initial concentrations of 1.6, 4.8, and 16 μM, 100 μL) and reference (120 μL) solutions were centrifuged at 10000 and 16000 rpm for at least 24 h at each speed until sedimentation equilibrium was attained. This was determined by overlaying scans taken at 2 h intervals. At sedimentation equilibrium, the final absorbance versus radial position profile was collected at 238 nm and 20 °C, with a step size of 0.001 cm and 10 averages. Sedimentation equilibrium data were globally fitted to a three discrete species model and a monomer−dimer−tetramer self-association model with mass conservation constraints using the program SEDPHAT (*36*), which is also available from www.analyticalultracentrifugation.com.

Size-Exclusion Chromatography. Samples of DHDPS (100 μL, 16 μM) were loaded onto a Sephadex 200 10/300 column (GE Healthcare) and eluted at 0.5 mL·min^{-1} with 20 mM Tris-HCl and 150 mM NaCl, pH 8.0 at 4 °C. The absorbance at 280 nm was monitored, and 0.25 mL fractions were collected and assayed for activity using the *o*-aminobenzaldehyde assay (*9*). Twenty microliters of each fraction were added to 100 μL of buffer containing 100 mM Tris-HCl, 2 mM pyruvate, 2 mM (*S*)-ASA, and 1 mg·mL^{-1} *o*-aminobenzaldehyde, pH 8.0. Assays were incubated at 37 °C for 10−30 min before 50 μL of 10% (w/v) trichloroacetic acid was added. Relative activity was determined by measuring the absorbance at 595 nm.

Liquid Chromatography Mass Spectrometry (Denaturing). Samples of freshly prepared DHDPS-Y107W were analyzed using a Waters 2790 HPLC system and a Waters 996 photodiode array (PDA) detector coupled in parallel to a Micromass LCT mass spectrometer equipped with an electrospray ionization (ESI) probe. The cone voltage was 35 V. A Phenomenex column (Luna C5, 5 μm, 2.00 × 150 mm) was used, eluted at 200 μL·min^{-1} with a solvent gradient from 100% water (0.5% formic acid) to 100% acetonitrile. Data were processed with MassLynx 4.0 software.

Nanoflow Electrospray Ionization Mass Spectrometry (Nondenaturing). Wild-type DHDPS and DHDPS-Y107W were incubated in 2% β-mercaptoethanol at 37 °C for 30 min before buffer exchange into 200 mM ammonium acetate (pH 7.0) using Bio-Spin6 columns (Bio-Rad). Nanoflow electrospray ionization mass spectrometry (nESI MS) was performed on an LCT instrument (Waters/Micromass) modified for high mass operation and optimized for the transmission of noncovalent complexes (*37*). Two microliters of DHDPS solution (monomer concentration 1.5−2.2 μM) were infused into the mass spectrometer from gold-coated borosilicate capillaries prepared in-house as described previously (*38*).

The following experimental parameters were applied: capillary voltage 1.5 kV, sample cone 100−200 V, extraction cone 0 V, analyzer pressure 6.4 mbar, and ToF analyzer pressure (2−2.1) × 10^{-6} mbar. Data were processed with MassLynx 4.0 software (Waters/Micromass) and are shown with minimal smoothing and without background subtraction. The mass spectrometer was calibrated using cesium iodide solution (100 mg·mL^{-1}).

Circular Dichroism (CD) Spectroscopy. CD spectroscopic data were generated using a Jasco J-815 circular dichroism spectrophotometer. DHDPS spectra were collected at a concentration of 16 μM enzyme in buffer containing 50 mM Na_2HPO_4, pH 8.0. Wavelength scans were collected at 20 °C using a 2 mm path-length cuvette, 1.0 nm bandwidth, 0.1 nm step size, and a 1 s averaging time. Temperature scans were monitored at 220 nm, and data were collected at 0.5 °C intervals between 20 and 80 °C with a 1 s averaging time. Cuvettes were stoppered during temperature scans to prevent evaporation.

Differential Scanning Fluorimetry. Thermal shift assays were carried out as described previously (*39*). A 25 μL aliquot of solution containing 16 μM protein and 50 mM Na_2HPO_4, pH 8.0, and 10× Sypro-orange dye (Invitrogen) was added to the wells of a 96-well thin-wall PCR plate (Bio-Rad). The plates were sealed and heated in an iCycler iQ real time PCR detection system (Bio-Rad) from 20 to 80 °C in increments of 0.2 °C, with 10 s dwell time. Fluorescence changes in the wells of the plate were monitored simultaneously with a charge-coupled device (CCD) camera. The wavelengths for excitation and emission were 490 and 575 nm, respectively. Experiments were carried out in triplicate for each condition.

Kinetics. Y107W DHDPS activity was measured using a coupled assay with DHDPR, as previously described (*2*). Typical assays (1 mL) contained 100 mM HEPES, pH 8.0, 0.16 mM NADPH, 50 μg·mL^{-1} DHDPR, 0.16−0.64 μM DHDPS-Y107W, and varying concentrations of (*S*)-ASA, pyruvate, and (*S*)-lysine. The assays were initiated by the addition of DHDPS, and the temperature was kept constant at 30 °C by the use of a circulating water bath. Stock solutions of (*S*)-ASA, NADPH, pyruvate, and (*S*)-lysine were prepared fresh for each experiment, and care was taken to ensure that an excess of DHDPR was present in the assays. Initial rate data were analyzed using nonlinear regression software (OriginLab, Northampton, MA) and fitted to the ping-pong model, which is also known as the double displacement enzyme mechanism (*40*). For lysine inhibition assays, data were fitted to equations for mixed partial inhibition or noncompetitive partial inhibition, as described previously (*10*).

RESULTS AND DISCUSSION

Structural Features of the Mutant Enzyme. To determine if the secondary structure of DHDPS-Y107W had been altered in aqueous solution, CD spectra were collected for the mutant and compared to those of the wild-type enzyme. DHDPS and DHDPS-Y107W exhibited almost identical spectra (Supporting Information Figure S1), with a broad

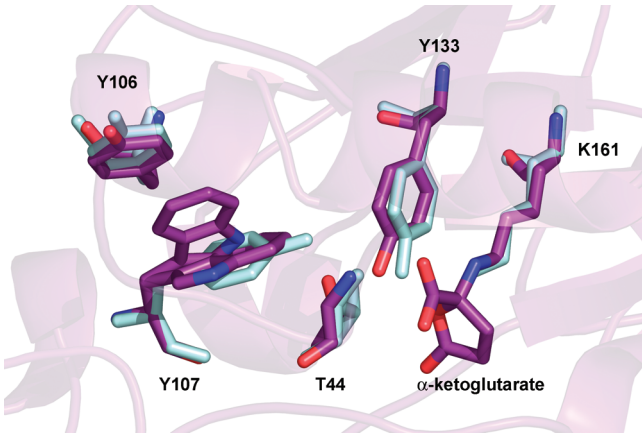

FIGURE 2: Structure of DHDPS-Y107W (purple) overlaid with the wild-type DHDPS (1YXC, shown in blue) showing some of the residues involved in catalysis.

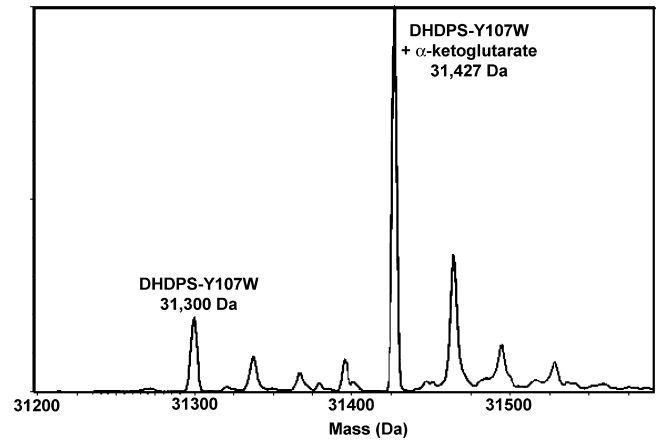

FIGURE 3: Denaturing LCMS of DHDPS-Y107W reveals peaks matching the free enzyme and a species corresponding to the mass of the protein with a covalent cyclic α-ketoglutarate adduct.

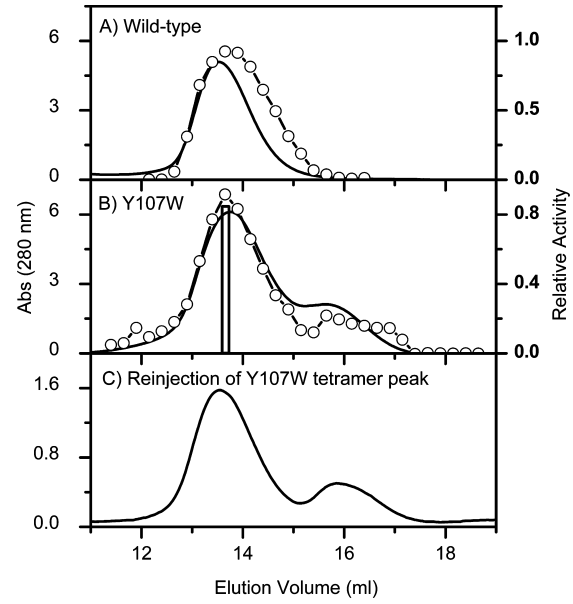

FIGURE 4: Size-exclusion chromatography shows that whereas the wild-type is almost entirely tetrameric (A), DHDPS-Y107W exists as a mixture of tetramer and monomer in solution (B). Reinjection of the tetramer peak indicated in panel B also indicates a mixture of tetramer and monomer in solution (C). Solid lines show the absorbance at 280 nm, whereas the dashed lines with circles show the relative activity of collected fractions.

minimum between 208 and 222 nm, which is consistent with the $(\alpha/\beta)_8$-barrel structure of the protein and the CD spectra previously observed for DHDPS (*16*).

Crystals of DHDPS-Y107W were grown under the same conditions as previously used for the native and mutated enzymes (*10, 17*), and the structure was determined by molecular replacement, using the wild-type structure from the Protein Data Bank, entry 1YXC (*10*). The final model contained 292 amino acid residues in each chain, with two chains in the asymmetric unit, from which the tetramer was generated by crystallographic symmetry. No significant changes were observed in the tertiary or quaternary structure of DHDPS-Y107W (Figure 2), with the enzyme existing as a homotetramer and each monomer containing a $(\alpha/\beta)_8$ barrel with the active site situated at the center of the $(\alpha/\beta)_8$ barrel in each monomer.

Consistent with its postulated catalytic role, Tyr107 is under conformational strain in all structures of wild-type and mutant versions of *E. coli* DHDPS (*10, 16, 17, 22, 28*), as is the equivalent Tyr131 residue in *N. sylvestris* DHDPS (*18*). This residue is located at the tight-dimer interface, and the side chain reaches into the active site of the other monomer to participate in the catalytic triad motif (*10*). When the DHDPS-Y107W structure was checked with PROCHECK, all residues fell within allowed regions of the Ramachandran plot, except for Trp107, which is under conformational strain and does not have well-defined density for the side chain, suggesting a degree of flexibility. In our final model, Trp107 has been modeled in two alternative conformations.

Similar to the DHDPS-Y107F mutant (*10*) and the dimer interface mutants (*22*), α-ketoglutarate is observed to be covalently attached to atom NZ of Lys161 and in its cyclic form for DHDPS-Y107W. This species binds adventitiously *in vivo* to DHDPS-Y107W and is carried through all protein purification steps. The *B* values of this moiety are only slightly higher than those of adjacent residues, with the exception of Arg138 and Trp107, which have noticeably higher *B* values compared to the wild-type enzyme, indicating that α-ketoglutarate is present in close to full occupancy. Denaturing ESI-TOF mass spectrometry of freshly prepared DHDPS-Y107W showed a peak at 31300 Da and a further peak at 31427 Da (Figure 3), corresponding to the covalent cyclic α-ketoglutarate adduct, as was seen also for DHDPS-L197Y (*22*).

When Tyr107 was previously mutated to phenylalanine, a surrogate water molecule was found in the active site close to where the hydroxyl of Tyr107 would have been located (*10*). However, the increased size of tryptophan in DHDPS-Y107W compared to tyrosine or phenylalanine means that there is no room for a water molecule to replace the hydroxyl group, although, paradoxically, there is room for the Trp107 to be disordered.

Gel Filtration Shows Disruption to the Quaternary Structure. Whereas the crystal structure of DHDPS-Y107W revealed a tetrameric enzyme, size-exclusion chromatography showed that there was disruption to the quaternary structure in solution. Compared to the wild-type enzyme, which showed a single peak corresponding to the tetrameric species (Figure 4A), two distinct peaks were observed for DHDPS-Y107W, corresponding to monomeric and tetrameric species (Figure 4B). The absorbance at 280 nm showed good

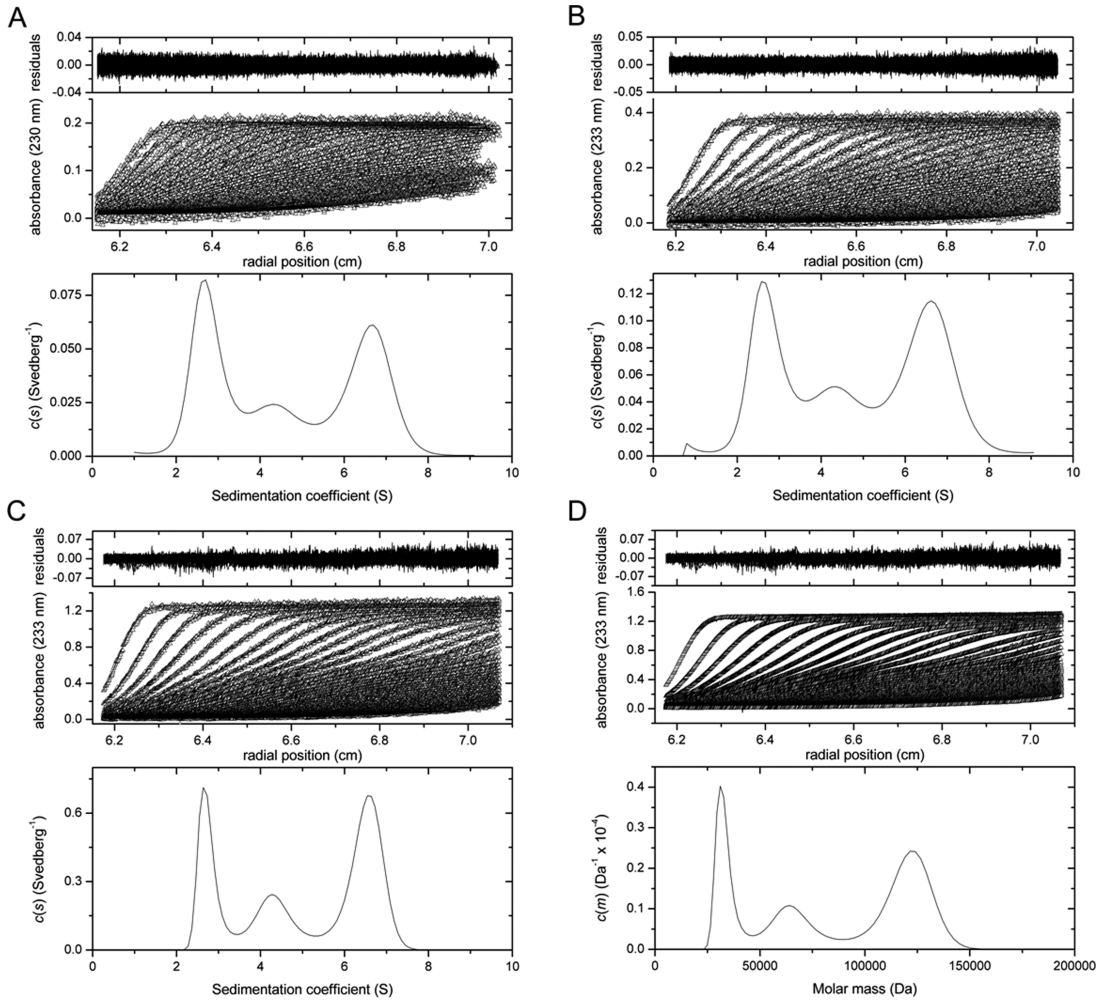

FIGURE 5: (A−C) Sedimentation velocity analysis of DHDPS-Y107W at three concentrations fitted to a continuous sedimentation coefficient [$c(s)$] distribution model (*34*): 1.6 μM (A), 4.8 μM (B), and 16 μM (C). The data were collected at 45000 rpm. (D) Continuous-mass [$c(M)$] distribution for DHDPS-Y107W (data from (C) at 16 μM) showing the masses of the three oligomeric species. For each panel, the top plot shows the residuals for the continuous size-distribution best fit shown in the middle panel, and the bottom panel shows the distribution of species. Also, for each panel (A−D) every third scan is shown for clarity, and the nonlinear least squares regression best fits to the $c(s)$ or $c(M)$ models are represented as solid lines. The resulting rmsd and the runs test-Z values are as follows: (A) rmsd = 0.006, runs-Z = 2.7; (B) rmsd = 0.006, runs-Z = 4.4; (C) rmsd = 0.009, runs-Z = 18; (D) rmsd = 0.009, runs-Z = 18.

correlation with the enzyme activity, showing that the late eluting species was active DHDPS enzyme. Reapplication of the tetrameric peak to the column again produced two peaks with similar ratios as originally observed (Figure 4C), suggesting that DHDPS-Y107W exists as a mixture of monomer and tetramer in solution.

Analytical Ultracentrifugation Reveals the Presence of Monomeric, Dimeric, and Tetrameric Species. To confirm the size-exclusion chromatography results, sedimentation velocity and sedimentation equilibrium experiments were carried out. Initial experiments utilized the sedimentation velocity technique at three protein concentrations: 1.6, 4.8, and 16 μM. The absorbance versus radial position data (Figure 5A−C) show three sedimenting boundaries, suggesting that three oligomeric populations of DHDPS-Y107W exist in aqueous solution. This was confirmed by fitting the data to a continuous size-distribution model, which showed three species with standardized sedimentation coefficients of 2.75, 4.46, and 6.83 S (Table 2). When the 16 μM data were fitted to a continuous mass [$c(M)$] distribution (Figure 5D) the resulting best fit showed three distinct peaks, corresponding to masses of 31, 64, and 123 kDa, which agree well with the expected masses of the DHDPS-Y107W monomer (M_r = 31293 Da), dimer, and tetramer, respectively. The calculated frictional ratio (f/f_0) for each oligomer suggests that the shapes of the monomer, dimer, and tetramer species in solution are similar, with f/f_0 values ranging from 1.22 to 1.26, which are consistent for globular proteins (Table 2). In contrast, no peaks corresponding to the dimeric species had been observed during gel filtration chromatography analyses (Figure 4). This is most likely due to the reduced resolution of gel filtration, which is unable to resolve the

Table 2: Hydrodynamic Properties of DHDPS-Y107W Oligomers Calculated by Sedimentation Velocity Analyses

oligomeric species	$s_{20,w}$ (S)[a]	f/f_0[b]	a/b[c]
monomer	2.75	1.24	2.55
dimer	4.46	1.22	2.22
tetramer	6.83	1.26	2.79

[a] Standardized sedimentation coefficient calculated from the ordinate maximum of each peak shown in the $c(s)$ distribution best fit at 16 mM (Figure 6C). [b] Frictional ratio calculated from the vbar method (*34*). [c] Axial ratio assuming a prolate ellipsoid calculated using the vbar method (*34*).

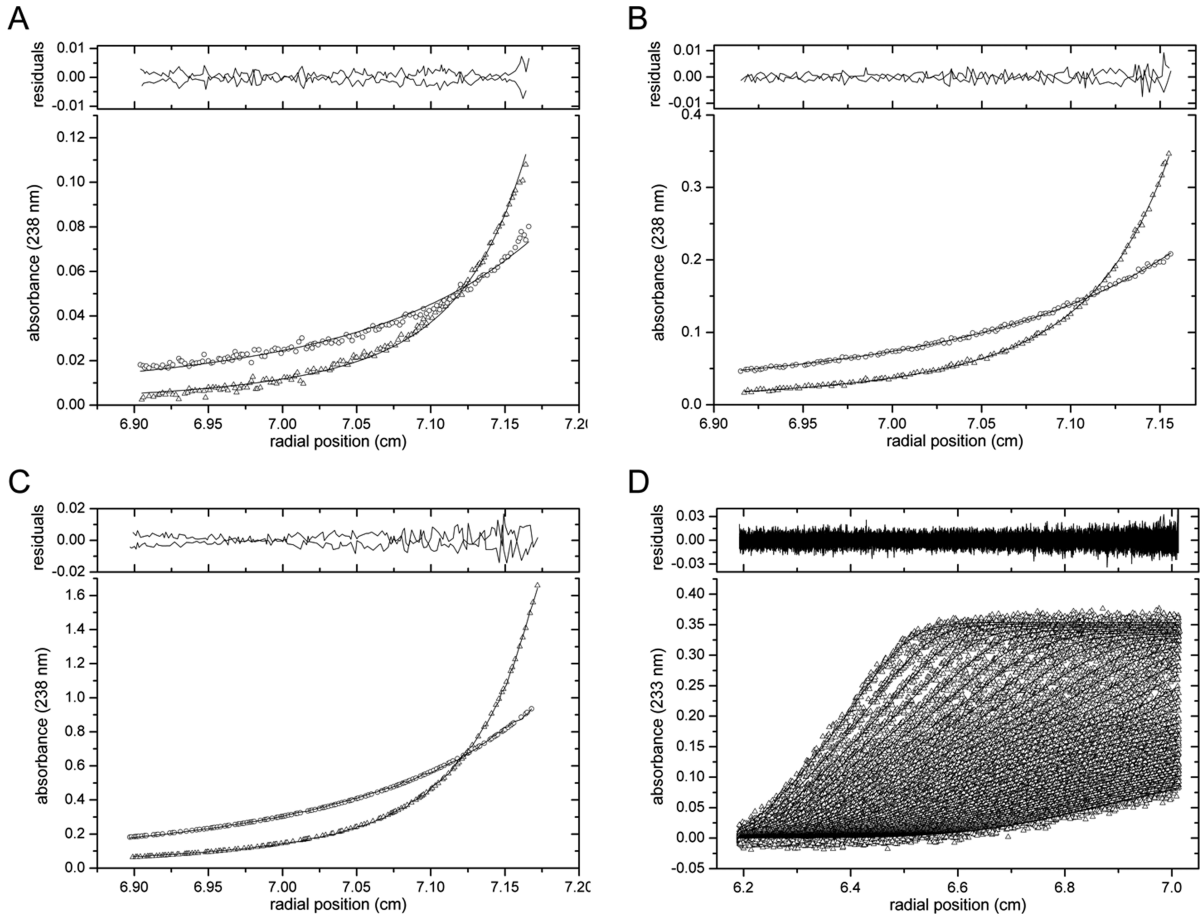

FIGURE 6: Sedimentation equilibrium data obtained at 10000 rpm (○) and 16000 rpm (▽) overlaid with the global nonlinear regression best fit to a model describing three discrete species with a global reduced χ^2 value of 4.0×10^{-1} (A−C). The experiment was conducted with initial protein concentrations of 1.6 μM (A), 4.8 μM (B), and 16 μM (C) and included sedimentation velocity data collected at 4.8 μM (D, and also shown in Figure 5B). The best fit was to a model describing three discrete species of mass 30861 Da (2.6 S), 66568 Da (4.6 S), and 131476 Da (6.8 S), which agrees with DHDPS-Y107W monomer, dimer, and tetramer, respectively. Residuals plots resulting from the fits are shown above the fit.

relatively low proportion of dimeric species relative to the tetrameric and monomeric species.

In order to confirm the oligomeric identity of the species shown in Figure 5 and provide insight into thermodynamic and, in combination with sedimentation velocity studies, kinetic self-associating properties, sedimentation equilibrium experiments were undertaken at multiple concentrations and speeds. The data were fitted to several models, including a nonequilibrium mixture of three species and a monomer−dimer−tetramer equilibrium model. The global nonlinear least squares best fit to sedimentation equilibrium data at DHDPS-Y107W concentrations of 1.6 μM (Figure 6A), 4.8 μM (Figure 6B), and 16 μM (Figure 6C) and sedimentation velocity data generated at 4.8 μM (Figure 6D) were obtained to a discrete species model comprised of monomer (2.6 S), dimer (4.6 S), and tetramer (6.8 S) (Figure 6). The best fit yielded a global reduced χ^2 value of 0.403 and is consistent with the continuous size-distribution analyses reported in Figure 5. These data were also fitted to a monomer−dimer−tetramer self-association model (Supporting Information Figure S2), which yielded sedimentation coefficients of 2.9 S (monomer), 3.5 S (dimer), and 7.0 S (tetramer), a global reduced χ^2 value of 0.431, and the thermodynamic and rate constants reported in Table 3. Not surprisingly, this fit indicates that the oligomeric species are in a very slow equilibrium, which explains why the sedimentation velocity data fit well to a $c(s)$ distribution model (Figure 5) and also why the global nonlinear least squares best fit was obtained to a nonequilibrium mixture of monomers, dimers, and tetramers (Figure 6).

Table 3: Thermodynamic and Kinetic Parameters Resulting from the Global Least Squares Best Fit to a Monomer−Dimer−Tetramer Self-Association Model[a]

parameter	best fit value
rate constants	
$k_{on}^{1\rightarrow2}$	15 $M^{-1}\cdot s^{-1}$
$k_{on}^{2\rightarrow4}$	1.1×10^3 $M^{-1}\cdot s^{-1}$
$k_{off}^{2\rightarrow1}$	1.5×10^{-4} s^{-1}
$k_{off}^{4\rightarrow2}$	2.0×10^{-4} s^{-1}
thermodynamic constants	
$K_D^{2\rightarrow1}$	9.9 μM
$K_D^{4\rightarrow2}$	0.18 μM

[a] The best fit to this model resulted in a global reduced χ^2 of 0.431.

Together, the results of sedimentation velocity and sedimentation equilibrium studies suggest that the presence of the Trp107 side chain in the mutant enzyme disrupts the tight-dimer interface sufficiently such that the equilibrium constant for the dissociation of dimers to monomers becomes weaker than that for tetramers to dimers (Table 3). Furthermore, this point mutation at the tight-dimer interface also appears to affect the weak-dimer interface, since the tetramer−dimer dissociation constant of DHDPS-Y107W

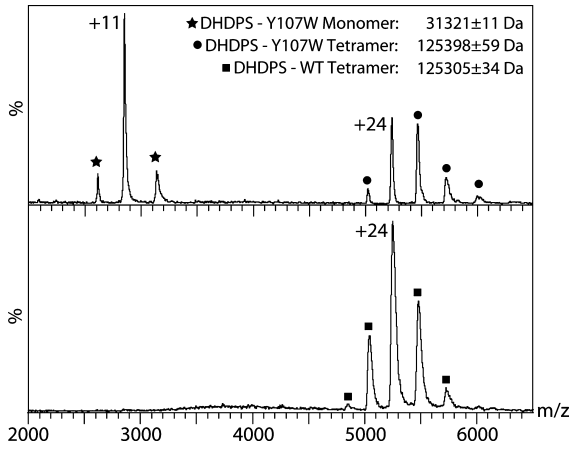

FIGURE 7: ESI mass spectra of the DHDPS-Y107W mutant (top) and wild type (bottom) under nondissociating MS conditions preserving noncovalent interactions. The wild-type enzyme exists only as a tetramer (charge states observed +26 to +22), whereas DHDPS-Y107W exists as a mixture of tetramer (charge states observed +25 to +21) and monomer (charge states observed +10 to +12). To obtain more accurate mass measurements, more stringent MS conditions were required as the poor complex desolvation required to observe no gas-phase dissociated monomer resulted in reduced mass measurement accuracy.

[$K_D^{4\rightarrow2} = 0.18$ μM (Table 3)] is significantly weaker than for the wild-type enzyme [$K_D^{4\rightarrow2} = 0.076$ μM (*21*)].

Nondenaturing Mass Spectrometry Also Reveals the Presence of a Monomeric Species. Following the observation by sedimentation studies that DHDPS-Y107W exists as a nonequilibrium mixture of oligomers (Figures 5 and 6), nondenaturing ESI-MS experiments were performed with DHDPS-Y107W and wild-type DHDPS. Wild-type DHDPS enzyme was examined under MS conditions optimized to maintain noncovalent interactions and revealed peaks corresponding to the +26 to +22 charge states of the tetrameric enzyme. Studies of the DHDPS-Y107W mutant under the same conditions showed, in addition to a charge state distribution corresponding to the tetramer, the presence of a species with lower *m/z* values corresponding to the +10 to +12 charge states of monomeric DHDPS-Y107W (Figure 7). Under more stringent MS conditions improved mass accuracy for each tetramer species was achieved, and gas-phase dissociated monomer yielded accurate masses for both wild-type and DHDPS-Y107W monomers (31306 ± 14 and 31321 ± 11 Da, respectively).

Interestingly, no dimeric species of DHDPS-Y107W are observed in the nondenaturing mass spectrum shown in Figure 7 (top). This suggests that the dimer observed in solution by sedimentation studies (Figures 5 and 6), which is stabilized largely by hydrophobic contacts at the loose dimer interface (*17, 28*), is destabilized during the ionization process in the mass spectrometer. This is consistent with the hydrophobic interactions at the interface being weakened in the gas phase, as has previously been noted (*41*). The lack of detected dimer in the gas phase may also reflect the low concentration (i.e., 1.5 μM) and/or differing buffer conditions employed in the ESI-MS experiment relative to the analytical ultracentrifugation studies.

To confirm that the presence of the free DHDPS-Y107W monomer in solution was not an artifact of solution or mass spectrometry conditions, equimolar solutions of DHDPS-Y107W and carbon- and nitrogen-labeled wild-type enzyme were mixed and infused into the mass spectrometer from the same capillary under identical instrument parameters. The free monomer species of DHDPS-Y107W was still observed under a range of conditions (Supporting Information Figure S3), confirming that it is not a result of the experimental conditions. No incorporation of either wild-type DHDPS or DHDPS-Y107W monomers into the other tetrameric species was detected when the solutions were incubated at 22 or 4 °C for up to 240 h. Further subunit exchange experiments were carried out to measure exchange between labeled and unlabeled wild-type enzyme and between labeled and unlabeled DHDPS-Y107W enzyme. These experiments confirmed the absence of exchange for either form of enzyme over a 43 h incubation period at room temperature. Measurements over a longer time period were unable to be made, due to the reduced stability of DHDPS-Y107W, which was no longer soluble after 48 h.

Together, the ESI-MS and sedimentation experiments indicate that the oligomers of DHDPS-Y107W reside in a nonequilibrium mixture that undergoes very slow subunit exchange. This result contrasts with the initial gel filtration data, which showed that reinjection of either of the monomeric or tetrameric peaks gave a mixture of monomeric and tetrameric species, suggesting that the dissociation−reassociation processes are relatively quick and equilibrium is reestablished fairly quickly. One possibility for this difference is that interactions occur between the enzyme and the gel matrix that promote the exchange of subunits.

The DHDPS-Y107W Mutant Has a Lower Melting Point Than the Wild-Type Enzyme. To determine the effect of the Y107W mutation on the thermal stability of DHDPS, CD spectroscopy and differential scanning fluorimetry were used to measure changes in the melting temperature. A CD spectrometer was used to monitor the ellipticity at 220 nm while the enzyme was incubated up to 80 °C (Figure 7). A sigmoidal curve fitted the data well and provided an indication of the temperature at which half of the change occurred, defined here as the apparent melting temperature (T_m^{app}). The CD spectrum of the wild-type enzyme underwent a dramatic increase in ellipticity, with a T_m^{app} of 61 °C, as previously observed (*15*), whereas DHDPS-Y107W showed similar increase in ellipticity and a considerably lower T_m^{app} of 47 °C. This indicates that DHDPS-Y107W has significantly lower thermal stability than the wild-type enzyme.

We sought to confirm this by using differential scanning fluorimetry, a technique that measures the thermal unfolding of proteins in the presence of a fluorescent dye (*39, 42*). In these experiments, the enzymes were incubated up to 80 °C in the presence of Sypro-orange, a dye which is normally quenched in aqueous solutions but binds to the exposed hydrophobic interior regions of the unfolding protein, leading to an increase in fluorescence emission (*42*). Both enzymes showed an increase in fluorescence as the temperature was increased, followed by a decrease in fluorescence, which is most likely due to precipitation of the denatured protein. Analysis of the data showed that the wild-type enzyme had a maximum point of inflection at 59 °C, whereas DHDPS-Y107W showed reduced heat stability, with a maximum point of inflection at 47 °C. These values show good agreement to those obtained by CD analyses.

Together, the CD and differential scanning fluorimetry results confirm that DHDPS-Y107W has reduced thermal

Table 4: Kinetic Parameters for DHDPS Determined Using the Ping-Pong Kinetic Mechanism

	DHDPS-Y107W (this study)	wild type (*20*)	DHDPS-Y107F (*20*)
K_m(pyruvate) (mM)	1.5 ± 0.2	0.26	0.16
K_m((*S*)-ASA) (mM)	0.39 ± 0.04	0.11	0.58
V_{max} (s^{-1})	6.5 ± 0.4	124	10.8

stability compared to the wild-type enzyme, which is consistent with the partially disrupted quaternary structure. Previous studies have shown that quaternary structure has a large effect on thermal stability, with thermophilic versions of the triosephosphate isomerase enzyme existing as a tetramer, rather than the dimeric enzyme found in other organisms (*43, 44*).

Enzyme Kinetics. Initial rate data from freshly prepared DHDPS-Y107W fitted the ping-pong kinetic mechanism (Table 4), in which one substrate (pyruvate) binds first, followed by the binding of the second substrate, in this case (*S*)-ASA. The maximal rate was 6.5 (±0.4) s^{-1}, which is reduced compared to the wild-type enzyme rate of 124 s^{-1} but similar to that of the DHDPS-Y107F rate of 10.8 s^{-1} (*20*) and faster than that of dimeric mutant enzymes, which have rates of 1−2 s^{-1} (*22*). DHDPS-Y107W had a Michaelis constant for pyruvate of 1.5 (±0.2) mM, which is much higher than that of the wild-type DHDPS (0.26 mM) and DHDPS-Y107F (0.16 mM) (*20*) and similar to that of the dimeric variants (1.11 and 0.68 mM) (*22*). Similarly, the Michaelis constant for (*S*)-ASA for DHDPS-Y107W (0.39 ± 0.04 mM) was higher than the wild-type (0.11 mM) and dimeric variants (0.18 and 0.15 mM) but less than the DHDPS-Y107F mutant (0.58 mM).

The reduced activity of DHDPS-Y107W is consistent with the important role shown by Tyr107 in shuttling protons to and from the active site to the solvent. The apparent increases in Michaelis constants for both pyruvate and (*S*)-ASA are consistent with the presence of a covalent adduct at the active site (*22*). This diminution in catalytic competency appears to occur to a much greater extent for the DHDPS-Y107W enzyme than for the DHDPS-Y107F mutant enzyme, which is consistent with the previous observation of a water molecule located at the position normally occupied by the tyrosine hydroxyl group (*20*). No water molecule is observed at this site in the structure of DHDPS-Y107W, and the steric bulk of the tryptophan residue reduces the effectiveness of Tyr133 to function as both a general acid and a general base in the catalytic mechanism and possibly to shuttle protons to and from the bulk solvent. Thus, once the α-ketoglutarate is displaced from the active site by pyruvate (*22*) the catalysis is more efficient in DHDPS-Y107F than DHDPS-Y107W, due to the presence of the water molecule (*20*). These measurements of enzyme kinetics are complicated by the nonequilibrium nature of DHDPS-Y107W in solution and the likelihood that there will be distinct populations of tetrameric, dimeric, and monomeric enzyme in solution. Despite this, the data gave a good fit to the models used.

Inhibition by (S)-Lysine. Inhibition by (*S*)-lysine is reduced in DHDPS-Y107W, compared to the wild-type enzyme (Table 3). There is a similar pattern of partial mixed inhibition with respect to (*S*)-ASA and partial noncompetitive inhibition with respect to pyruvate (*10*). There is good correlation of the lysine inhibition data with the Michaelis−Menten data, with K_m^{app} values similar to the K_m values. Similarly, the K_{ES} value of 0.69 mM for (*S*)-lysine binding to the ES complex is comparable to the value of 0.60 mM for (*S*)-lysine inhibition with respect to (*S*)-ASA.

Table 5: Like the Wild-Type Enzyme, DHDPS-Y107W Shows Partial Mixed Inhibition by (*S*)-Lysine with Respect to (*S*)-ASA and Partial Noncompetitive Inhibition by (*S*)-Lysine with Respect to Pyruvate[a]

		DHDPS-Y107W	wild type (*10*)
vs pyruvate	V'/V_{max}	0.26 ± 0.13	0.05 ± 0.02
	K_m^{app} (mM)	1.5 ± 0.2	0.14 ± 0.01
	K_E (mM)	2.7 ± 0.7	3.9 ± 1.4
	K_{ES} (mM)	0.69 ± 0.12	0.18 ± 0.16
vs (*S*)-ASA	V'/V_{max}	0.27 ± 0.03	0.09 ± 0.02
	K_m^{app} (mM)	0.39 ± 0.03	0.12 ± 0.01
	K_E (mM)	0.60 ± 0.09	0.32 ± 0.03

[a] V' represents the maximal activity in the presence of saturating activity. V_{max} is the maximal activity in the absence of inhibition. K_E and K_{ES} are the inhibition constants for I binding to the E and ES complexes, respectively.

Although the inhibition constant for (*S*)-lysine binding is similar for both DHDPS-Y107W and wild-type DHDPS, DHDPS-Y107W still retains over 25% of uninhibited activity, even at high inhibitor concentrations (Table 5), compared to the wild-type enzyme retaining less than 10% of normal activity (*10*). This is consistent with the (*S*)-lysine binding to DHDPS-Y107W, but only to the tetrameric form, as the monomeric form lacks the lysine binding site, which lies at the interface of the two subunits of the tight dimer. It has previously been observed that inhibition of the dimeric variant of DHDPS by (*S*)-lysine was unchanged (*22*). The residual activity is also consistent with the tetramer−dimer−monomer equilibration being slower than the rate of enzyme turnover, as found by analytical ultracentrifugation and mass spectrometry.

CONCLUSIONS

For the *E. coli* DHDPS enzyme, we have recently demonstrated that quaternary structure is critical for function (*22*). Although X-ray crystallographic studies show that there is little change to the tertiary and quaternary structure of the DHDPS-Y107W enzyme in the crystal form, we show that this single amino acid substitution is sufficient to weaken both the tight- and weak-dimer interfaces of the tetramer, resulting in a mutant enzyme that exists as a mixture of monomers, dimers, and tetramers in solution. Consistent with other active site mutants previously characterized (*10*), the catalytic ability of DHDPS-Y107W was significantly attenuated, with a reduction in catalytic rate and increase in the Michaelis constants. In addition, weaker binding of substrates and loss of conformational rigidity allows α-ketoglutarate to adventitiously bind to the active site of the mutant enzyme. Inhibition by (*S*)-lysine was reduced, with a significant degree of activity remaining at high inhibitor concentrations, and is hypothesized to be due to a lack of binding by (*S*)-lysine to the monomeric enzyme in solution. Thus, the tetrameric quaternary structure of DHDPS is critical to controlling specificity, heat stability, and intrinsic activity.

Our studies of the dimeric enzyme concluded that increased flexibility in the dimeric enzyme, relative to wild-type DHDPS, hinders catalysis, providing a selective advantage for association of two dimers to form a tetramer. Another form of DHDPS, the naturally occurring dimer from

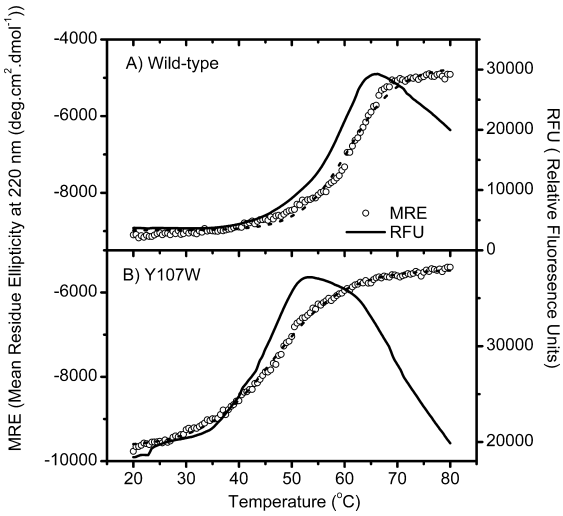

FIGURE 8: CD spectroscopy and differential scanning fluorimetry reveals that DHDPS-Y107W has reduced thermal stability compared to the wild-type enzyme. Mean residue ellipticity at 220 nm (symbols) was measured using a Jasco J-815 CD spectrometer and fitted to a sigmoid (dotted line). Relative fluorescence with the Sypro-orange dye (solid line) was measured using a Bio-Rad iQ5 RT-PCR detector.

methicillin-resistant *S. aureus*, uses an alternative method of reducing dynamic fluctuations by having an increased surface area at the tight-dimer interface (*19*). The results presented here provide clues as to the activity of the ancient monomeric enzyme, which may have had impaired Michaelis constants for both substrates and not be inhibited by (*S*)-lysine. Further work is underway to create a fully monomeric enzyme to test these hypotheses.

ACKNOWLEDGMENT

We thank Jackie Healy for ubiquitous technical support.

SUPPORTING INFORMATION AVAILABLE

An overlay of the CD spectra for wild-type and Y107W DHDPS, the results of fitting equilibrium data to a monomer−dimer−tetramer self-association model, and ESI mass spectra of wild-type and Y107W DHDPS under identical solution and MS conditions. This material is available free of charge via the Internet at http://pubs.acs.org.

REFERENCES

1. Cox, R., Sutherland, A., and Vederas, J. (2000) Bacterial diaminopimelate metabolism as a target for antibiotic design. *Bioorg. Med. Chem. 8*, 843–871.
2. Coulter, C. V., Gerrard, J. A., Kraunsoe, J. A. E., and Pratt, A. J. (1999) *Escherichia coli* dihydrodipicolinate synthase and dihydrodipicolinate reductase: kinetic and inhibition studies of two putative herbicide targets. *Pestic. Sci. 55*, 887–895.
3. Miflin, B., Napier, J., and Shewry, P. (1999) Improving plant product quality. *Nat. Biotechnol. 17*, 13–14.
4. Blickling, S., Renner, C., Laber, B., Pohlenz, H., Holak, T., and Huber, R. (1997) Reaction mechanism of *Escherichia coli* dihydrodipicolinate synthase investigated by X-ray crystallography and NMR spectroscopy. *Biochemistry 36*, 24–33.
5. Galili, G. (1995) Regulation of lysine and threonine synthesis. *Plant Cell 7*, 899–906.
6. Ghislain, M., Frankard, V., and Jacobs, M. (1990) Dihydrodipicolinate synthase of *Nicotiana sylvestris*, a chloroplast-localized enzyme of the lysine pathway. *Planta 180*, 480–486.
7. Frisch, D. A., Gengenbach, B. G., Tommey, A. M., Sellner, J. M., Somers, D. A., and Myers, D. E. (1991) Isolation and characterization of dihydrodipicolinate synthase from maize. *Plant Physiol. 96*, 444–452.
8. Wallsgrove, R. M., and Mazelis, M. (1981) Spinach leaf dihydrodipicolinate synthase: partial purification and characterization. *Biochemistry 20*, 2651–2655.
9. Yugari, Y., and Gilvarg, C. (1965) The condensation step in diaminopimelate synthesis. *J. Biol. Chem. 240*, 4710–4716.
10. Dobson, R. C., Valegard, K., and Gerrard, J. A. (2004) The crystal structure of three site-directed mutants of *Escherichia coli* dihydrodipicolinate synthase: Further evidence for a catalytic triad. *J. Mol. Biol. 338*, 329–339.
11. Bartlett, A., and White, P. (1986) Regulation of the enzymes of lysine biosynthesis in *Brevibacterium lactofermentum* NCTC 9602 during vegetative growth. *J. Gen. Microbiol. 132*, 3169–3177.
12. Stahly, D. (1969) Dihydrodipicolinate synthase of *Bacillus licheniformis*. *Biochim. Biophys. Acta 191*, 439–451.
13. Cremer, J., Eggeling, L., and Sahm, H. (1990) Cloning the *dapA dapB* cluster of the lysine-secreting bacterium *Corynebacterium glutamicum*. *Mol. Gen. Genet. 229*, 478–480.
14. Tosaka, O., and Takinami, K. (1978) Pathway and regulation of lysine biosynthesis in *Brevibacterium lactofermentum*. *Agric. Biol. Chem. 42*, 95–100.
15. Pearce, F. G., Perugini, M. A., McKerchar, H. J., and Gerrard, J. A. (2006) Dihydrodipicolinate synthase from *Thermotoga maritima*. *J. Biochem. 143*, 617–623.
16. Dobson, R. C. J., Devenish, S. R. A., Turner, L. A., Clifford, V. R., Pearce, F. G., Jameson, G. B., and Gerrard, J. A. (2005) Role of arginine 138 in the catalysis and regulation of *Escherichia coli* dihydrodipicolinate synthase. *Biochemistry 44*, 13007–13013.
17. Mirwaldt, C., Korndorfer, I., and Huber, R. (1995) The crystal structure of dihydrodipicolinate synthase from *Escherichia coli* at 2.5 Å resolution. *J. Mol. Biol. 246*, 227–239.
18. Blickling, S., Beisel, H. G., Bozic, D., Knablein, J., Laber, B., and Huber, R. (1997) Structure of dihydrodipicolinate synthase of *Nicotiana sylvestris* reveals novel quaternary structure. *J. Mol. Biol. 274*, 608–621.
19. Burgess, B. R., Dobson, R. C. J., Griffin, M. D. W., Jameson, G. B., Parker, M. W., Gerrard, J. A. and Perugini, M. A. 2008. Structure and evolution of a novel dimeric enzyme from a clinically-important bacterial pathogen. *J. Biol. Chem. 283*, 27598–27603.
20. Dobson, R. C. J., Valegard, K., and Gerrard, J. A. (2004) The crystal structure of three site-directed mutants of *Escherichia coli* dihydrodipicolinate synthase: Further evidence for a catalytic triad. *J. Mol. Biol. 338*, 329–339.
21. Perugini, M. A., Griffin, M. D. W., Smith, B. J., Webb, L. E., Davis, A. J., Handman, E., and Gerrard, J. A. (2005) Insight into the self-association of key enzymes from pathogenic species. *Eur. J. Biophys. 34*, 469–476.
22. Griffin, M. D. W., Dobson, R. C. J., Pearce, F. G., Antonio, L., Whitten, A. E., Liew, C. K., Mackay, J. P., Trewhella, J., Jameson, G. B., Perugini, M. A., and Gerrard, J. A. (2007) Evolution of quaternary structure in a homotetrameric protein. *J. Mol. Biol. 380*, 691–703.
23. Bradford, M. (1976) A rapid and sensitive method for the quantitation of microgram quantities of protein utilizing the principle of protein-dye binding. *Anal. Biochem. 72*, 248.
24. Roberts, S. J., Morris, J. C., Dobson, R. C. J., and Gerrard, J. A. (2003) The preparation of (*S*)-aspartate semi-aldehyde appropriate for use in biochemical studies. *Bioorg. Med. Chem. Lett. 13*, 265–267.
25. Dobson, R. C. J., Gerrard, J. A., and Pearce, F. G. (2004) Dihydrodipicolinate synthase is not inhibited by its substrate, (*S*)-aspartate beta-semialdehyde. *Biochem. J. 377*, 757–762.
26. Pflugrath, J. W. (1999) The finer things in X-ray diffraction data collection. *Acta Crystallogr., Sect. D: Biol. Crystallogr. 55*, 1718–1725.
27. Navaza, J., and Saludjian, P. (1997) AMoRe: An automated molecular replacement program package. *Methods Enzymol. 276*, 581–594.
28. Dobson, R. C. J., Griffin, M. D. W., Jameson, G. B., and Gerrard, J. A. (2005) The crystal structures of native and (*S*)-lysine bound dihydrodipicolinate synthase from *Escherichia coli* with improved resolution show new features of biological significance. *Acta Crystallogr., Sect. D: Biol. Crystallogr. 61*, 1116–1124.
29. Bailey, S. (1994) The CCP4 suite—programs for protein crystallography. *Acta Crystallogr., Sect. D: Biol. Crystallogr. 50*, 760–763.

30. Emsley, P., and Cowtan, K. (2004) Coot: model-building tools for molecular graphics. *Acta Crystallogr., Sect. D: Biol. Crystallogr. 60*, 2126–2132.
31. Lamzin, V. S., and Wilson, K. S. (1997) Automated refinement for protein crystallography. *Methods Enzymol. 277*, 269–305.
32. Kleywegt, G. J., and Jones, T. A. (1996) xdlMAPMAN and xdlDATAMAN—Programs for reformatting, analysis and manipulation of biomacromolecular electron-density maps and reflection data sets. *Acta Crystallogr., Sect. D: Biol. Crystallogr. 52*, 826–828.
33. Laskowski, R. A., Macarthur, M. W., Moss, D. S., and Thornton, J. M. (1993) Procheck—a program to check the stereochemical quality of protein structures. *J. Appl. Crystallogr. 26*, 283–291.
34. Schuck, P. (2000) Size-distribution analysis of macromolecules by sedimentation velocity ultracentrifugation and Lamm equation modeling. *Biophys. J. 78*, 1606–1619.
35. Laue, T. M., Shah, D. B., Ridgeway, T. M., and Pelletier, S. L. (1992) in *Analytical ultracentrifugation in biochemistry and protein science*, pp 90—125, The Royal Society of Chemistry, Cambridge.
36. Vistica, J., Dam, J., Balbo, A., Yikilmaz, E., Mariuzza, T. A., Rouault, P., and Schuck, P. (2004) Sedimentation equilibrium analysis of protein interactions with global implicit mass conservation constraints and systematic noise decomposition. *Anal. Biochem. 326*, 234–256.
37. Sobott, F., Hernandez, H., McCammon, M. G., Tito, M. A., and Robinson, C. V. (2002) A tandem mass spectrometer for improved transmission and analysis of large macromolecular assemblies. *Anal. Chem. 74*, 1402–1407.
38. Nettleton, E. J., Sunde, M., Lai, Z. H., Kelly, J. W., Dobson, C. M., and Robinson, C. V. (1998) Protein subunit interactions and structural integrity of amyloidogenic transthyretins: Evidence from electrospray mass spectrometry. *J. Mol. Biol. 281*, 553–564.
39. Neisen, F. H., Berglund, H., and Vedadi, M. (2007) The use of differential scanning fluorimetry to detect ligand interactions that promote protein stability. *Nat. Protoc. 2*, 2212–2221.
40. Cornish-Bowden, A. (1999) *Fundamentals of enzyme kinetics*, 2nd ed., Portland Press Ltd., London.
41. Daniel, J. M., Friess, S. D., Rajagopalan, S., Wendt, S., and Zenobi, R. (2002) Quantitative determination of noncolvalent binding interactions using soft ionization mass spectrometry. *Int. J. Mass Spectrom. 216*, 1–27.
42. Ericsson, U. B., Hallberg, B. M., DeTitta, G. T., Dekker, N., and Nordlund, P. (2006) Thermofluor-based high-throughput stability optimization of proteins for structural studies. *Anal. Biochem. 357*, 289–298.
43. Walden, H., Bell, G. S., Russell, R. J. M., Siebers, B., Hensel, R., and Taylor, G. L. (2001) Tiny TIM: A small, tetrameric, hyperthermostable triosephosphate isomerase. *J. Mol. Biol. 306*, 745–757.
44. Maes, D., Zeelen, J. P., Thanki, N., Beaucamp, N., Alvarez, M., Thi, M. H. D., Backmann, J., Martial, J. A., Wyns, L., Jaenicke, R., and Wierenga, R. K. (1999) The crystal structure of triosephosphate isomerase (TIM) from *Thermotoga maritima*: A comparative thermostability structural analysis of ten different TIM structures. *Proteins 37*, 441–453.

BI801094T